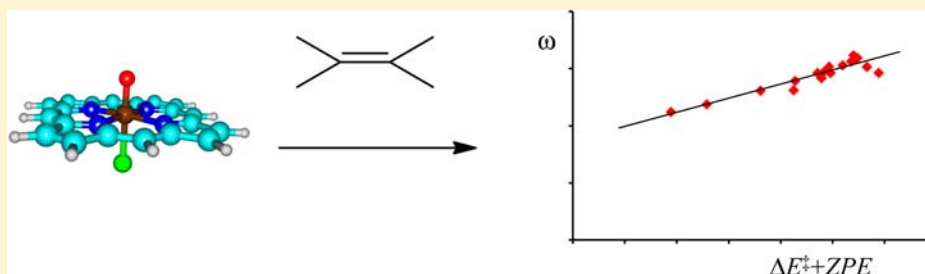


Rationalization of the Barrier Height for *p*-Z-styrene Epoxidation by Iron(IV)-Oxo Porphyrin Cation Radicals with Variable Axial LigandsDevesh Kumar,^{*,†} Reza Latifi,^{*,‡,§} Suresh Kumar,[†] Elena V. Rybak-Akimova,[§] Mala A. Sainna,[‡] and Sam P. de Visser^{*,‡}[†]Department of Applied Physics, School of Physical Sciences, Babasaheb Bhimrao Ambedkar University, Vidya Vihar, Rae Bareilly Road, Lucknow 226-025, India[‡]Manchester Institute of Biotechnology and School of Chemical Engineering and Analytical Science, University of Manchester, 131 Princess Street, Manchester M1 7DN, U.K.[§]Department of Chemistry, Tufts University, Medford, Massachusetts 02155, United States

S Supporting Information



ABSTRACT: A versatile class of heme monooxygenases involved in many vital functions for human health are the cytochromes P450, which react via a high-valent iron(IV) oxo heme cation radical species called Compound I. One of the key reactions catalyzed by these enzymes is C=C epoxidation of substrates. We report here a systematic study into the intrinsic chemical properties of substrate and oxidant that affect reactivity patterns. To this end, we investigated the effect of styrene and para-substituted styrene epoxidation by Compound I models with either an anionic (chloride) or neutral (acetonitrile) axial ligand. We show, for the first time, that the activation enthalpy of the reaction is determined by the ionization potential of the substrate, the electron affinity of the oxidant, and the strength of the newly formed C–O bond (approximated by the bond dissociation energy, BDE_{OH}). We have set up a new valence bond model that enables us to generalize substrate epoxidation reactions by iron(IV)-oxo porphyrin cation-radical oxidants and make predictions of rate constants and reactivities. We show here that electron-withdrawing substituents lead to early transition states, whereas electron-donating groups on the olefin substrate give late transition states. This affects the barrier heights in such a way that electron-withdrawing substituents correlate the barrier height with BDE_{OH} , while the electron affinity of the oxidant is proportional to the barrier height for substrates with electron-donating substituents.

■ INTRODUCTION

An important class of enzymes in human physiology are the cytochromes P450, which are a large set of heme enzymes involved in the biodegradation and metabolism of toxic compounds in the liver.¹ These enzymes utilize molecular oxygen on a heme center in a catalytic cycle that uses two electrons and two protons to generate an iron(IV) oxo heme cation-radical active species called Compound I (CpdI).² This species is the active oxidant of the P450 enzymes and reacts with substrates via, for instance, aliphatic and aromatic hydroxylation, double-bond epoxidation, N-dealkylation, and sulfoxidation.³ Because of its versatility in substrate activation, the group of enzymes has attracted interest from the biotechnological and pharmaceutical industries, although the intricate details of its catalytic mechanism and reactivity with substrates are still poorly understood. The epoxidation of olefins is a common reaction in P450 enzymes for a variety of

important bioprocesses in the body including the activation of unsaturated fatty acids.⁴ As a result, substrate epoxidation by P450 isozymes is well studied for a wide range of (non)natural substrates.⁵ For instance, the reactions were shown to be highly enantioselective, whereby the *cis*- β -methylstyrene substrate gave an 89:11 epoxide product ratio of the 1*S*,2*R* form over the 1*R*,2*S* form.⁶

Because CpdI is a very versatile oxidant, many studies investigated synthetic analogues and models in substrate oxidation.⁷ A number of these biomimetic studies focused on double-bond epoxidation mechanisms, and one of the most common substrates in these studies is styrene. Thus, a series of styrene epoxidation studies with a CpdI mimic and various axial ligands gave rate constants that were proportional to its

Received: February 27, 2013

Published: July 3, 2013

electron-donating ability.⁸ Green and co-workers⁹ characterized the axial-ligand effect as arising from changes in the pK_a values of the oxo group, which was confirmed with density functional theory (DFT) calculations on model complexes.¹⁰

Experimental studies reported rate constants for styrene epoxidation by synthetic iron(IV) oxo complexes: $[\text{Fe}^{\text{IV}}(\text{O})(\text{TPFP}^{\bullet+})\text{X}]^{0/+}$ with $\text{TPFP} = \text{meso-tetrakis-(pentafluorophenyl)porphyrinato}$ and $\text{X} = \text{Cl}^-$ or NCCH_3 .¹¹ In an intriguing set of experiments, it was shown that the reaction of $[\text{Fe}^{\text{IV}}(\text{O})(\text{TPFP}^{\bullet+})\text{NCCH}_3]^+$ with ethylbenzene gave aromatic hydroxylation products, whereas the one using $[\text{Fe}^{\text{IV}}(\text{O})(\text{TPFP}^{\bullet+})\text{Cl}]$ as an oxidant led to benzylic hydroxylation instead; hence, the axial ligand in iron(IV)-oxo porphyrins seems to affect the product distributions in the reaction processes and the regioselectivity of aromatic versus aliphatic hydroxylation.¹¹ The two oxidants with chloride versus acetonitrile as the axial ligand also gave differences in styrene epoxidation using para-substituted styrene derivatives. The work identified a correlation between the rate constant of styrene epoxidation with the ρ^+ Hammett factor, but the slopes were different for the CpDI models with anionic versus neutral axial ligands. The fundamental nature of this axial-ligand effect and how it affects the reaction mechanisms, rate constants and product distributions of iron(IV)-oxo porphyrins is unknown and, therefore, warrants a computational study. Thus, to gain insight into the effect of axial ligands on the reactivity of iron(IV)-oxo porphyrins with olefins, we have done a DFT study of the activation barriers using a selection of para-substituted styrenes as substrates and CpDI models with meso-substituted porphyrin.

Fujii and co-workers did a systematic investigation into the redox potentials of $[\text{Fe}^{\text{IV}}(\text{O})(\text{TMP}^{\bullet+})\text{X}]^{n+}$ with $\text{TMP} = 5,10,15,20\text{-tetramesitylporphyrinate}$ and X an axial ligand that is either anionic or neutral.¹² They found a positive $E_{1/2}$ shift upon binding of an anionic axial ligand that was virtually constant for a range of ligands. By contrast, binding of neutral ligands, such as imidazole, gave redox potentials in line with those found for peroxidases corresponding to a negative $E_{1/2}$ shift. They then replaced the TMP group with a meso-substituted porphyrin ligand with electron-withdrawing groups, which led to an increase of the $E_{1/2}$ values. Currently, it is not clear what factors determine the redox potentials of iron porphyrins and whether there is a relationship with catalysis. Therefore, to gain insight into the effect of meso substitution on the intrinsic chemical properties of the oxidant and the subsequent catalysis of substrates, we decided to include this study in the present work.

The model we chose for our studies presented here is given in Figure 1 and is based on the system used in ref 11. The basic features of the oxidant are an iron(IV) oxo group embedded in a protoporphyrin IX (Por) without side chains and with either

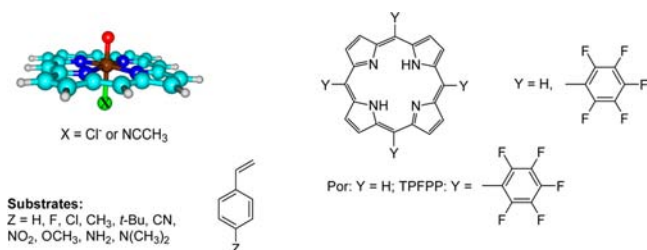


Figure 1. Oxidants and substrates used in this work.

chloride or acetonitrile as the axial ligand: $[\text{Fe}^{\text{IV}}(\text{O})(\text{Por}^{\bullet+})\text{X}]^{0/+}$ with $\text{X} = \text{Cl}^-$ or NCCH_3 . In addition, we also investigated a more elaborate model that uses pentafluorophenyl substituents on the meso position of the porphyrin ring, i.e., TPFP. Substrate epoxidation was studied using a range of *p*-Z-substituted styrenes with $\text{Z} = \text{H}, \text{F}, \text{Cl}, \text{CH}_3, t\text{-Bu}, \text{CN}, \text{NO}_2, \text{OCH}_3, \text{NH}_2,$ and $\text{N}(\text{CH}_3)_2$. We show that para substitution affects the ionization potential of the substrate and its electron-donating ability, which leads to changes in the activation barrier of oxygen atom transfer. Although we reported a detailed analysis of substrate epoxidation by iron(IV)-oxo porphyrins before,¹⁰ the systematic study described here goes beyond that of the previous work and highlights the differences in reactivity of substrates with electron-donating versus electron-withdrawing substituents. Moreover, a new model is presented that correlates with the obtained reactivity trends.

METHODS

The study presented here uses DFT methods, as implemented in the *Jaguar*, *Gaussian03*, and *Gaussian09* program packages.¹³ All geometries are the result of a full geometry optimization, whereby all degrees of freedom are minimized. A subsequent analytical frequency calculation characterized the structures as local minima (with real frequencies only) or first-order saddle points with one imaginary frequency for the correct mode. The hybrid B3LYP method¹⁴ was employed throughout in combination with the Los Alamos-type LACVP basis set on iron and 6-31G on the rest of the atoms (BS1) for the geometry optimizations and frequencies.¹⁵ Energies were then improved by single-point calculations with a triple- ζ -type basis set on iron (LACV3P+) and 6-311+G* on the rest of the atoms (BS2). Benchmark studies against experimental data reproduced free energies of activation using these methods to within 3 kcal mol⁻¹.¹⁶ Previously, we calculated a full potential energy profile for substrate hydroxylation by an iron(IV)-oxo porphyrin cation-radical system at UB3LYP/BS2 and obtained relative energies within a few tenths of a kilocalorie per mole for local minima and first-order saddle points along a reaction mechanism compared to those obtained at UB3LYP/BS2//UB3LYP/BS1; hence, the latter method was used here.¹⁷ Single-point calculations in a dielectric constant with $\epsilon = 37.5$ mimicking acetonitrile with a probe radius of 2.1 Å were performed in *Jaguar* using basis set BS2. Free energies reported here were calculated at 298 K temperature and 1 bar pressure and are based on the UB3LYP/BS2//UB3LYP/BS1 energies and corrected with zero-point energy (ZPE), thermal and entropic corrections from the frequency file, and solvent corrections from the single-point solvent calculation. Further corrections to the energy were made by performing single-point calculations with dispersion-corrected B3LYP, B3LYP-D, as implemented in *Jaguar*.¹⁸ For selected structures, we also did geometry optimizations and frequencies using UB3LYP-D/BS1 in *Jaguar*, although little changes in the optimized geometries were obtained.

We used two synthetic iron porphyrin models that are distinguished by the choice of the axial ligand, which was either chloride or acetonitrile. Note that $[\text{Fe}^{\text{IV}}(\text{O})(\text{Por}^{\bullet+})\text{Cl}]^0$ is overall charge neutral, while $[\text{Fe}^{\text{IV}}(\text{O})(\text{Por}^{\bullet+})\text{NCCH}_3]^+$ is positively charged. In our initial calculations, we used a bare porphyrin ring, whereby all side chains were replaced by hydrogen atoms. In a second set of calculations, we studied a TPFP ligand system. We studied styrene epoxidation using a selection of para-substituted styrene substrates, as described in Figure 1.

To ascertain that the results are not influenced by the DFT method chosen here, we ran a selection of single-point calculations using dispersion-corrected DFT¹⁸ and B3LYP with 15% HF exchange (designated as B3LYP*).¹⁹ As before,²⁰ these test calculations reproduced the trends obtained with the B3LYP method, so that the results give a systematic error, which does not affect our discussion and analysis because we are dealing with trends only here. Nevertheless, for comparison, we give here the results obtained for $\Delta E + \text{ZPE}$

(UB3LYP), $\Delta G + E_{\text{solv}}$ (UB3LYP), and $\Delta G + E_{\text{solv}} + E_{\text{disp}}$ (UB3LYP-D).

RESULTS

We started the work with a detailed study into the electronic properties of iron(IV) oxo complexes, the effects of axial versus equatorial ligands, and finally the reactivity patterns with a selection of para-substituted styrenes. Our models include $[\text{Fe}^{\text{IV}}(\text{O})(\text{Por}^{\bullet+})\text{X}]^{0/+}$, designated as 1_{X} , and $[\text{Fe}^{\text{IV}}(\text{O})(\text{TPFPP}^{\bullet+})\text{X}]^{0/+}$, designated as 2_{X} , with $\text{X} = \text{Cl}^-$ and NCCH_3 (Figure 1). Similar to previous studies on CpDI of P450 and biomimetic iron(IV)-oxo porphyrin complexes,²¹ all complexes have the same electronic ground state with four electrons in metal 3d-type orbitals and a radical on the porphyrin macrocycle. High-lying occupied molecular orbitals include the $\delta_{x^2-y^2}$ orbital, which is nonbonding, doubly occupied, and located in the plane of the porphyrin. Slightly higher in energy are two π_{FeO}^* orbitals (π_{xz}^* , π_{yz}^*) for the antibonding interaction of the metal $3d_{xz/yz}$ with $2p_{x/y}$ atomic orbitals on oxygen. Higher-lying and virtual are the $\sigma_{z^2}^*$ and σ_{xy}^* orbitals for the antibonding interactions along the Fe–O axis and between the Fe–N groups in the plane of the porphyrin ring. In addition, there is a radical on a porphyrin-type orbital that in D_{4h} symmetry has the label a_{2u} . The orbital occupation gives close-lying doublet and quartet spin states with configuration $\delta_{x^2-y^2}^2 \pi_{xz}^* \pi_{yz}^* a_{2u}^1$, whereby the two π^* electrons are either ferromagnetically or antiferromagnetically coupled to the a_{2u} electron in the quartet and doublet spin states. As a consequence, the two spin states are close in energy and the oxidant reacts via two-state-reactivity patterns on close-lying doublet and quartet spin state surfaces.²²

Figure 2 gives optimized geometries of ${}^4,21_{\text{X}}$ and ${}^4,22_{\text{X}}$ with $\text{X} = \text{Cl}^-/\text{NCCH}_3$, as calculated with DFT. Optimized geometries of ${}^4,21_{\text{X}}$ ($\text{X} = \text{Cl}^-/\text{NCCH}_3$) are almost identical with those reported before.²³ The Fe–O distances are short and typical for an iron(IV) oxo species and shorten somewhat with an axially ligated acetonitrile molecule compared to chloride. This is due to mixing of the a_{2u} and π^* orbitals in ${}^4,21_{\text{Cl}}$ with 3p atomic orbitals on the chloride ligand,²³ which brings the metal more inside the plane through the porphyrin ring. This type of mixing has been identified before as the key reason for the intrinsic electronic differences of CpDI in monooxygenases and peroxidases.²⁴ We did additional geometry optimizations of ${}^21_{\text{X}}$ ($\text{X} = \text{Cl}^-/\text{NCCH}_3$) at the UB3LYP-D/BS1 level of theory, which reproduced the UB3LYP/BS1 structures within 0.010 Å.

As can be seen, meso substitution of the porphyrin ring with pentafluorophenyl groups has little effect on the optimized geometries, and the Fe–O, Fe–Cl, and Fe–N_{ax} distances for structures 1 and 2 are almost the same. Note also that very little saddling is found for the $[\text{Fe}^{\text{IV}}(\text{O})(\text{TPFPP}^{\bullet+})\text{X}]$ structures. Not surprisingly, because the same molecular orbitals are singly occupied in the doublet and quartet spin-state structures, their geometries are virtually identical for each CpDI set of data. To establish whether the meso-pentafluorophenyl groups give electronic changes to the iron(IV) oxo species, we also show in Figure 2 the group spin densities (ρ), but only minor differences are observed between the data for structures 1 and 2.

Subsequently, we calculated styrene epoxidation using a range of para-substituted styrene derivatives. Before we discuss the results on the substituted styrenes, let us focus on the general overall mechanism first. All epoxidation reactions described in this work proceed with the same stepwise

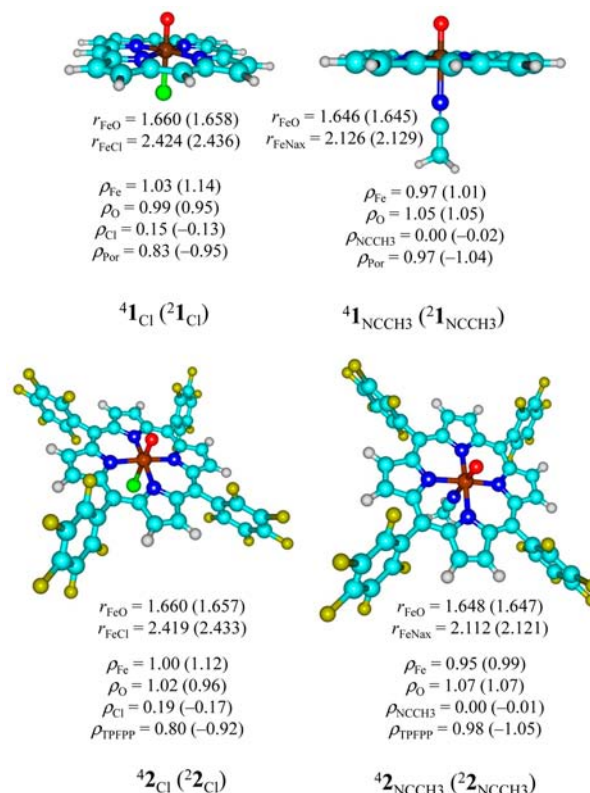


Figure 2. UB3LYP/BS1-optimized geometries of ${}^4,21_{\text{X}}$ and ${}^4,22_{\text{X}}$ in the gas phase with bond lengths in angstroms. Group spin densities are obtained at UB3LYP/BS2//UB3LYP/BS1 and are reported in atomic units.

mechanism that starts with the formation of a reactant complex between CpDI and substrate, **R**. As an example, we give the reaction profile for $[\text{Fe}^{\text{IV}}(\text{O})(\text{Por}^{\bullet+})\text{Cl}]$ with *p*-H-styrene in Figure 3 on the lowest doublet and quartet spin states. The spin multiplicity is given as a superscript, and in the subscript, we give the axial ligand (X) and the *p*-Z substituent of styrene. The mechanism resembles that found in earlier studies of substrate epoxidation of olefins by metal(IV) oxo oxidants^{23,25,26} and starts with an initial electrophilic addition of the oxo group to the double olefinic bond of styrene via a transition state $\text{TS}_{\text{X,Z}}$ to form a radical intermediate ($\text{I}_{\text{X,Z}}$), whereby the subscript X refers to the axial ligand, i.e., $\text{X} = \text{Cl}^-$ or AN (acetonitrile), and the subscript Z to the para substituent of styrene. In a final reaction step, a ring-closure transition state ($\text{TS}_{\text{r,c,Z}}$) leads to epoxide product complexes ($\text{P}_{\text{X,Z}}$). Optimized geometries obtained at UB3LYP-D/BS1 show little difference from those obtained at UB3LYP/BS1 (Figure 3).

Although the ring-closure barrier was calculated for a selection of chemical systems, in all cases its barrier was much smaller than the C–O bond-formation barrier via $\text{TS}_{\text{X,Z}}$; therefore, we will focus here on the rate-determining barrier only. In particular, in the quartet spin state, ring-closure barriers were located and found to be small, whereas in the doublet spin state, the ring closure was virtually barrierless. The origin of this difference is due to differences in electron-transfer processes in the ring-closure step, whereby on the doublet spin-state surface, the π_{xz}^* orbital is filled with an extra electron, while on the quartet spin state, a higher-lying and virtual $\sigma_{z^2}^*$ orbital is filled with one electron.^{26a} Energies obtained for the reaction of $[\text{Fe}^{\text{IV}}(\text{O})(\text{Por}^{\bullet+})\text{Cl}]$ with *p*-H-styrene are very similar to those

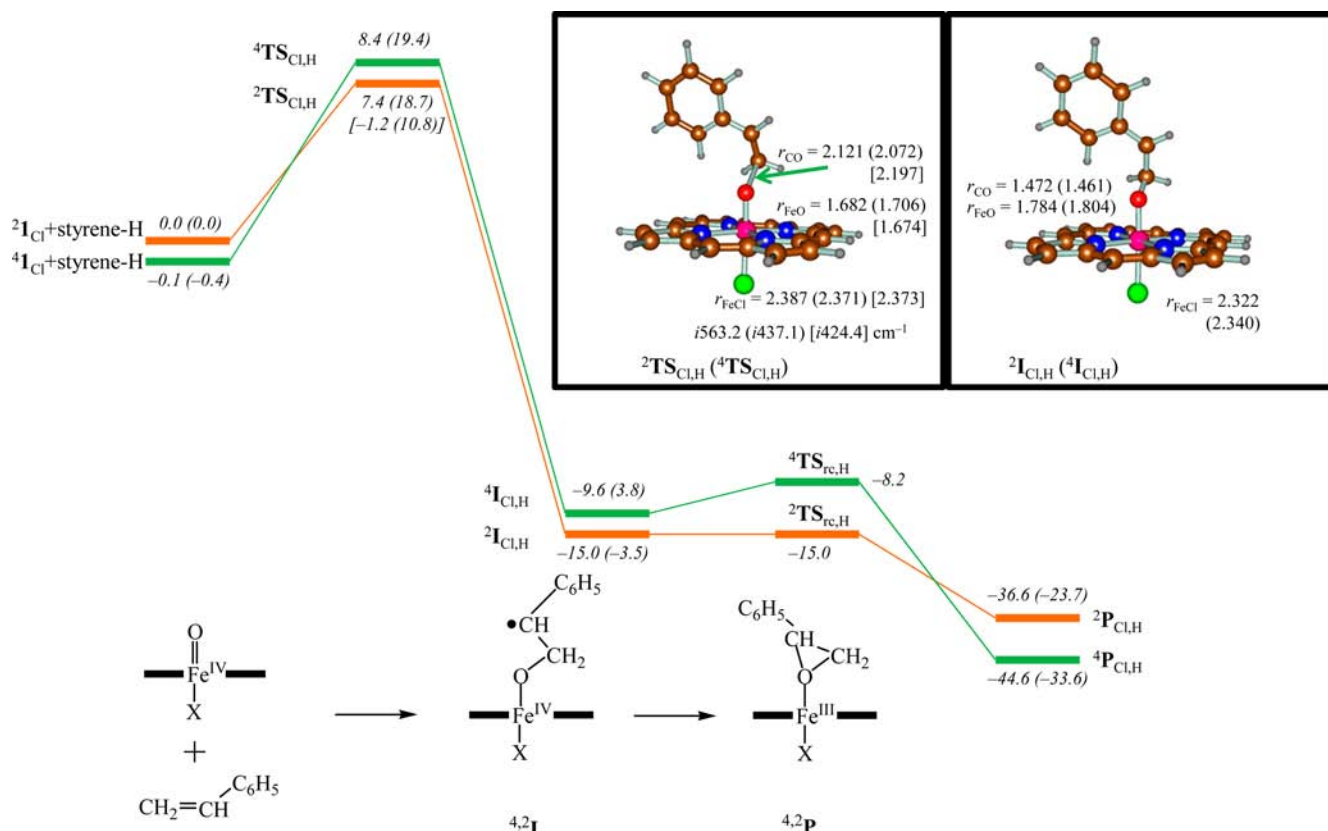


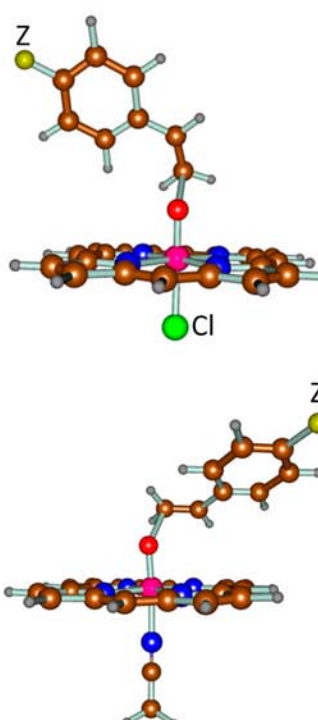
Figure 3. Potential energy profile of styrene epoxidation by $^{4,2}\text{I}_{\text{Cl}}$ as calculated with UB3LYP/BS2//UB3LYP/BS1. All energies are in kilocalories per mole relative to isolated reactants in the doublet spin state and include ZPE corrections. Also shown are optimized geometries of critical points with bond lengths in angstroms and the imaginary frequencies in the transition state in wavenumbers. Free energies are given in parentheses and include UB3LYP/BS2 energies corrected with thermal and entropic corrections at 298 K. Data in square brackets were obtained from a UB3LYP-D/BS2//UB3LYP-D/BS1 calculation.

reported before using $[\text{Fe}^{\text{IV}}(\text{O})(\text{Por}^{\bullet+})\text{SH}]$ as an oxidant.^{23,26b} That is not surprising because the $\text{p}K_{\text{a}}$ and electron affinity (EA) of $[\text{Fe}^{\text{IV}}(\text{O})(\text{Por}^{\bullet+})\text{X}]$, $\text{X} = \text{Cl}^-/\text{SH}^-$, are virtually the same. Geometries are typical for epoxidation structures from previous calculations for P450-catalyzed reaction mechanisms.^{25,26} In the transition state, the Fe–O bond elongates slightly with respect to reactants and further extends in the intermediate to 1.784 Å. At the same time, considerable shortening of the C–O distance occurs to a formally single bond in $^{4,2}\text{I}_{\text{Cl,H}}$ of 1.472 Å.

Subsequently, we investigated the reaction mechanisms of $[\text{Fe}^{\text{IV}}(\text{O})(\text{Por}^{\bullet+})\text{X}]^{0/+}$, $\text{X} = \text{Cl}^-$ or NCCCH_3 , with para-substituted styrene, and the optimized geometries of the transition states are given in Figure 4. Interestingly, structural differences are found between the two axially ligated oxidants, whereby the Cl^- -bound $\text{TS}_{\text{X,Z}}$ structures are with styrene in an upright position, whereas the acetonitrile-bound ones are more sideways-bound. Test calculations using an upright starting structure and an acetonitrile axial ligand, however, converged back to the sideways-bound structure instead, which implies that the upright structures are higher in energy for the axially ligated acetonitrile transition states. The differences in the substrate orientation affect the bond distances of the respective transition states. For instance, the bond-forming C–O distances vary from 2.017 to 2.241 Å for the transition states with $\text{X} = \text{Cl}^-$, whereas for $\text{X} = \text{NCCCH}_3$, distances between 2.083 and 2.439 Å are found. This implies that the barriers for the acetonitrile-ligated structures are somewhat earlier than the

ones for the chloride-bound systems. Although variations in the Fe–O and Fe–X distances are considerably smaller than those for the C–O distance, variations between the oxidant with chloride and acetonitrile ligands are also found.

The epoxidation barriers ($\text{TS}_{\text{Cl,Z}}$) range from 3.92 kcal mol⁻¹ for *p*-N(CH₃)₂-styrene to 7.40 kcal mol⁻¹ for *p*-H-styrene, i.e., vary by 3.48 kcal mol⁻¹ upon para substitution. With acetonitrile as the axial ligand, the lowest barrier is 10.56 kcal mol⁻¹ below isolated reactants for *p*-N(CH₃)₂-styrene, although it should be noted that the reactant complex is more stable than isolated reactants by 14.75 kcal mol⁻¹. Thus, the epoxidation barrier height varies by 20 kcal mol⁻¹ between *p*-N(CH₃)₂-styrene and *p*-NO₂-styrene for $\text{TS}_{\text{AN,Z}}$; hence, the substituent located at a distance of over 4 Å from the reaction center causes a rate constant change by a factor of ca. 10¹⁵ (estimated using transition state theory for an enthalpy-derived free energy change of 20 kcal mol⁻¹; the entropy of activation was not included in this estimate). The ordering of the barrier heights is virtually the same for the two oxidants studied, namely, $\text{Z} = \text{N}(\text{CH}_3)_2 < \text{NH}_2 < \text{OCH}_3 < \text{CH}_3/t\text{-Bu} < \text{F}/\text{Cl} < \text{CN} < \text{H}$. A plot of the barriers $^2\text{TS}_{\text{Cl,Z}}$ versus those calculated for $^2\text{TS}_{\text{AN,Z}}$ with the same methods gives a linear correlation; see Figure S27 in the Supporting Information (SI). Furthermore, calculations using a solvent model included give free energies of activation that follow the same trends as values found in the gas phase (Figure S28 in the SI). Inclusion of dispersion corrections on the solvent-corrected free energies of activation gives a further systematic change of the energetics, as shown in



Z	H	F	Cl	CH ₃	t-Bu	CN	NO ₂	OCH ₃	NH ₂	N(CH ₃) ₂
X = Cl ⁻										
r _{C-O}	2.121	2.107	2.090	2.142	2.143	2.053	2.017	2.163	2.232	2.241
r _{O-Fe}	1.682	1.684	1.685	1.680	1.680	1.689	1.692	1.679	1.674	1.674
r _{Fe-Cl}	2.387	2.386	2.385	2.390	2.389	2.383	2.382	2.392	2.399	2.401
imag	i563.2	i600.4	i641.0	i500.3	i500.1	i693.3	i697.8	i421.5	i269.4	i245.7
ΔE+ZPE	7.40	7.01	7.06	6.79	6.85	7.30	7.28	5.97	4.80	3.92
ΔG+E _{solv} +E _{disp}	13.8	11.2	11.9	9.4	11.3	12.7	11.8	10.1	6.5	-0.3
X = NCCH ₃										
r _{C-O}	2.187	2.178	2.160	2.244	2.272	2.117	2.083	2.305	2.430	2.439
r _{O-Fe}	1.668	1.673	1.677	1.659	1.653	1.692	1.703	1.653	1.648	1.646
r _{Fe-NCCH₃}	2.103	2.099	2.096	2.115	2.128	2.088	2.084	2.130	2.150	2.163
imag	i209.8	i220.3	i234.3	i181.1	i238.2	i274.4	i310.5	i147.8	i75.3	i66.0
ΔE+ZPE	3.55	4.15	4.66	1.39	1.25	8.30	9.44	-1.94	-7.11	-10.56
ΔG+E _{solv} +E _{disp}	6.3	8.7	10.7	5.7	7.7	24.8	27.0		4.9	-1.0

Figure 4. Optimized geometries of rate-determining transition states ${}^2\text{TS}_{X,Z}$ for the reaction of *p*-Z-styrene with ${}^2\text{I}_X$ ($X = \text{Cl}^-/\text{NCCH}_3$). Geometries optimized at UB3LYP/BS1 with bond lengths given in angstroms and the imaginary frequencies in wavenumbers. Also given are barrier heights ($\Delta E + \text{ZPE}$) for ${}^2\text{TS}_{X,Z}$ with energies calculated at UB3LYP/BS2//UB3LYP/BS1+ZPE relative to isolated reactants in kilocalories per mole and free energies of activation in a solvent ($\Delta G + E_{\text{solv}} + E_{\text{disp}}$) relative to ${}^2\text{RC}_{X,Z}$.

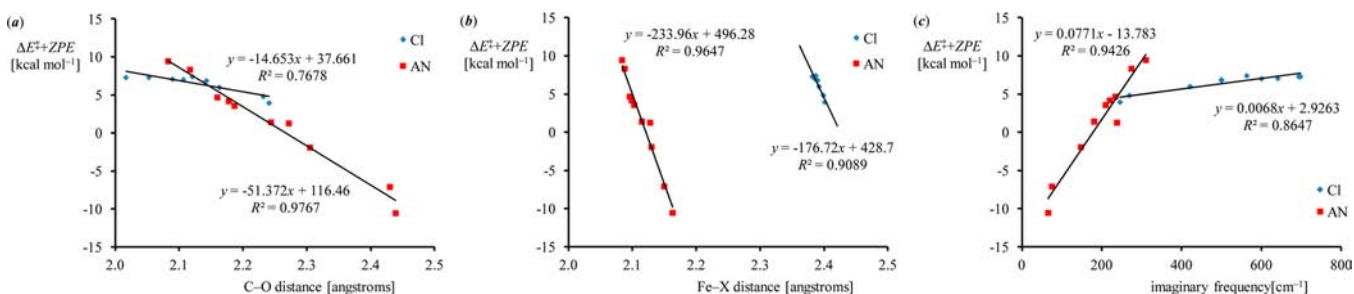


Figure 5. Analysis of the structural features of the transition states $\text{TS}_{X,Z}$ calculated at UB3LYP/BS1 as a function of the height of the epoxidation barrier with respect to the (a) C–O distance, (b) Fe–X distance, and (c) imaginary frequency in the transition state. Data are given for $X = \text{Cl}^-$ axial ligand (blue diamonds) and $X = \text{acetonitrile}$ (red squares).

Figures S29 and S30 in the SI. This highlights the fact that for the assignment of reactivity trends it does not matter whether $\Delta E + \text{ZPE}$, ΔG , $\Delta G + E_{\text{solv}}$ or $\Delta G + E_{\text{solv}} + E_{\text{disp}}$ energies are used. Because the enthalpies in a reaction mechanism are determined by the electronic changes of the reactants and we aim to establish the intrinsic chemical properties that determine the reactivity patterns, we will focus in the following on establishing trends through the $\Delta E + \text{ZPE}$ sets of data.

To understand the changes in the transition-state geometry between the para-substituted styrene substrates, we plot in Figure 5 a selection of bond distances versus the barrier height ($\Delta E^\ddagger + \text{ZPE}$) for the two CpDI models with either a chloride or an acetonitrile axial ligand. Figure 5a shows the distance of the C–O bond that is formed in the process versus the barrier height. An almost perfect linear correlation ($R^2 = 0.98$) is obtained for the acetonitrile-ligated transition states, and a

satisfactory linear correlation is found for the chloride-ligated system. Thus, a drop in the C–O bond length of 0.224 Å is found between the weakest epoxidating substrate (*p*-NO₂-styrene) and the strongest one [*p*-N(CH₃)₂-styrene] using a chloride axial ligand, whereas the difference between these substrates is 0.256 Å for an axially ligated acetonitrile molecule. This implies that the para substituent of styrene has a single possibly electrostatic effect on the C–O bond-formation step and, consequently, the barrier height of the reaction. To further ascertain that the optimized geometries and barrier heights are reproducible, we reoptimized a selection of TS structures with UB3LYP-D/BS1. Thus, ${}^2\text{TS}_{\text{AN,CN}}$ and ${}^2\text{TS}_{\text{Cl,CN}}$ give Fe–O distances of 1.683 and 1.680 Å and C–O distances of 2.131 and 2.107 Å, respectively. These values are close to those given in Figure 4 calculated at the UB3LYP/BS1 level of theory.

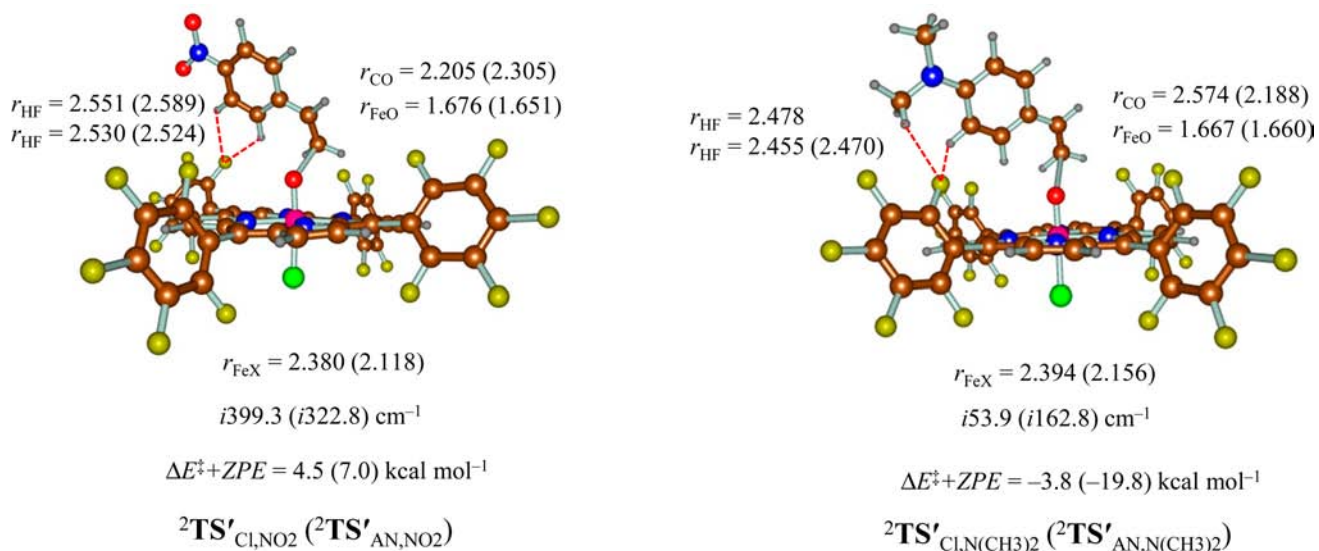


Figure 6. Optimized geometries of epoxidation transition states ${}^2\text{TS}'_{\text{X,Z}}$ for the reaction of 2_{X} ($\text{X} = \text{Cl}^-/\text{NCCH}_3$) with p -Z-styrene. Bond lengths are in angstroms and the values of the imaginary frequencies in wavenumbers.

We also investigated the correlations of the epoxidation barrier height with the Fe–O and Fe–X distances in the transition states, and indeed these correlations are linear as well. With a chloride axial ligand, modest Fe–O and Fe–Cl changes are seen throughout the series of -0.018 and $+0.019$ Å, respectively, between the outer ranges for p -NO₂-styrene and p -N(CH₃)₂-styrene. Much larger differences are found for the weakly bound acetonitrile system, where the Fe–NCCH₃ distance is elongated from 2.084 to 2.163 Å ($+0.079$ Å shift) between p -NO₂-styrene and p -N(CH₃)₂-styrene. Thus, the para substituent of styrene affects bond distances well over 5 Å from the catalytic center and weakens the metal-to-axial ligand distances of the Fe–Cl and Fe–NCCH₃ bonds dramatically.

Interestingly, even the value of the imaginary frequency gives a linear correlation with the barrier height, i.e., are that the para substituent of styrene affects the height as well as the width of the potential energy curve around the transition state. Because both the height and width of the barrier change linearly for our series of substrates, this means that the area under the curve could stay the same for these substrates. However, changes to the width of the potential energy curve may have important effects on, for instance, the kinetic isotope effects (KIEs) for a reaction.²⁷ Thus, a small imaginary frequency correlates with a broad and wide potential energy surface, whereas a large imaginary frequency implies a narrow and high peak. Tunnelling through a narrow and high peak should be easier than through a broad peak; therefore, KIEs associated with this reaction may be affected as well. It is interesting to note that the imaginary frequencies are substantially larger for $[\text{Fe}^{\text{IV}}(\text{O})(\text{Por}^{\bullet+})\text{Cl}]$ than for $[\text{Fe}^{\text{IV}}(\text{O})(\text{Por}^{\bullet+})\text{NCCH}_3]^+$; hence, the barriers for the latter oxidant will be much broader in shape. If this trend also applies to the hydrogen-atom-abstraction reaction, then this would imply that the calculations predict $[\text{Fe}^{\text{IV}}(\text{O})(\text{Por}^{\bullet+})\text{Cl}]$ to react with considerably larger KIEs for the replacement of hydrogen by deuterium atoms than $[\text{Fe}^{\text{IV}}(\text{O})(\text{Por}^{\bullet+})\text{NCCH}_3]^+$ with substrates. Indeed, Nam and co-workers reported differences in the KIE values for the two oxidants in aliphatic hydrogen-atom-abstraction reactions.¹¹

In a final set of calculations, we investigated the effect of meso substitution of the porphyrin ring on the electronic

properties of CpDI and the epoxidation of para-substituted styrenes. We selected the TPFPP ligand system with pentafluorophenyl groups on the meso position of the porphyrin and calculated styrene epoxidation using the TPFPP oxidant: $[\text{Fe}^{\text{IV}}(\text{O})(\text{TPFPP}^{\bullet+})\text{X}]^{0/+}$ with $\text{X} = \text{Cl}^-$ and NCCH_3 or 2_{X} . We studied styrene epoxidation for p -N(CH₃)₂-styrene and p -NO₂-styrene and compared the mechanism and energy profiles with those observed above for 1_{X} . Figure 6 displays optimized geometries of the epoxidation transition states $\text{TS}'_{\text{X,Z}}$ for the reaction of styrene with $2_{\text{X,Z}}$ with $\text{Z} = \text{NO}_2$ or $\text{N(CH}_3)_2$, as calculated with DFT methods.

Geometrically, there are striking differences between $\text{TS}_{\text{X,Z}}$ on the one hand, and $\text{TS}'_{\text{X,Z}}$ on the other hand. Thus, the epoxidation barriers with the TPFPP ligand system are characterized with long C–O and short Fe–O distances, which implies much earlier transition states along the potential energy surface. Furthermore, both acetonitrile- and chloride-ligated $\text{TS}'_{\text{X,Z}}$ structures are in the upright configuration, with a structure similar to the $\text{TS}_{\text{Cl,Z}}$ geometries reported in Figure 4. Probably, the stereochemical interactions with meso substituents prevent a substrate orientation analogous to $\text{TS}_{\text{AN,Z}}$ with a sideways attack on the oxo group. In addition, the structures are stabilized with hydrogen-bonding interactions of substrate C–H groups with the fluoride atoms from the TPFPP ligand and specifically those located in the ortho position of the meso substituent. As a consequence, both the reactant complexes and the transition states for epoxidation are considerably stabilized with respect to isolated reactants. Each transition state structure in Figure 6 is stabilized by at least two or three C–H...F hydrogen-bonding interactions with distances between 2.4 and 2.6 Å. F–H hydrogen-bonding interactions can be dramatic; for instance, trifluoromethanol as a solvent has been shown to lead to a considerable lowering of the epoxidation and halogenation barriers heights because of hydrogen-bonding and charge-transfer interactions.²⁸

Recent computational studies of dehydrogenation of cyclohexadiene by $[\text{Fe}^{\text{IV}}(\text{O})(\text{TPCPP}^{\bullet+})\text{Cl}]$ with TPCPP = *meso*-tetrakis(pentachlorophenyl)porphyrin also showed substrate stabilization due to weak hydrogen-bonding interactions of chloride atoms of the TPCPP ligand with C–H groups of the

approaching substrate.²⁹ These interactions were shown to be particularly strong for epoxidation barrier heights because of a closer approach to the oxidant compared to hydrogen-atom-abstraction reactions and lowered epoxidation barriers significantly.³⁰ In line with this, it is not surprising that we find a considerable lowering of the epoxidation barriers from 7.3 to 4.5 kcal mol⁻¹ for X = Cl/Z = NO₂, from 9.4 to 7.0 kcal mol⁻¹ for X = AN/Z = NO₂, from 3.9 to -3.8 kcal mol⁻¹ for X = Cl/Z = N(CH₃)₂, and from -10.6 to -19.8 kcal mol⁻¹ for X = AN/Z = N(CH₃)₂ upon replacement of the equatorial ligand from Por to TPFPP. The big changes in geometry for TS_{X,Z} compared to TS'_{X,Z} also affect the shape of the potential energy surface and the values of the imaginary frequencies. Both TS'_{Cl,NO₂} and TS'_{Cl,N(CH₃)₂} structures have lower imaginary frequencies than TS_{Cl,NO₂} and TS_{Cl,N(CH₃)₂}, whereas this is not the case for the axially ligated acetonitrile structures.

Thus, we report here the effect of meso substitution on the electronic and reactivity properties of iron(IV) oxo porphyrin cation-radical models. We find little changes in the electronic configuration of the various CpDI reactants. However, fluorine substituents on the meso position of TPFPP entice favorable electrostatic interactions with the approaching substrate and stabilize the epoxidation transition states. In the following, we will try to rationalize these observations.

DISCUSSION

In this work, we report a systematic set of epoxidations of substituted styrenes using four different oxidants, namely, **1**_{Cl}, **1**_{NCCH₃}, **2**_{Cl}, and **2**_{NCCH₃}. During the substrate epoxidation process, two electrons are transferred from the substrate to the oxidant, which is reduced from [Fe^{IV}(O)(Por^{•+})X] to [Fe^{III}(Por)X]. As a consequence, the EA of the oxidant and the ionization energy (IE) of the substrate should reflect the electron-transfer processes that take place. Indeed, several experimental studies found a correlation between the IE of substrates and the rate constant of substrate epoxidation and sulfoxidation.^{7s,31} So far, no experimental studies have been reported on the activation parameters of substrate epoxidation by synthetic biomimetic iron(IV)-oxo porphyrin cation-radical models, but the rate constants are expected to correlate with the activation enthalpies. In earlier work, we reported a systematic study of olefin epoxidation by iron(IV) oxo complexes and set up a model that predicts barrier heights from known ionization potentials. Although that correlation still applies, we generalize it further in this work using the data described here.

To understand the individual contributions of the oxidant and substrate to the reaction process, i.e., transition states, we will investigate those separately. Let us start with a discussion of the differences and a comparison between **1**_{Cl}/**2**_{Cl} and **1**_{NCCH₃}/**2**_{NCCH₃} in styrene epoxidation reactions and their corresponding EAs. Thus, as shown in Figure 2, the reactant complexes give little differences in the geometric and electronic features upon a change in the equatorial ligand from Por to TPFPP.

We calculated EA values of 79.4 kcal mol⁻¹ for **1**_{Cl}, 101.4 kcal mol⁻¹ for **2**_{Cl}, 148.7 kcal mol⁻¹ for **1**_{NCCH₃}, and 163.8 kcal mol⁻¹ for **2**_{NCCH₃} in the gas phase. Note here that, despite the fact that the valence orbital occupations and orbital shapes seem little influenced by the nature of the meso substituents of the porphyrin ring, actually the EA values increase by as much as 15.1–22.0 kcal mol⁻¹. This observation is in excellent

agreement with the electrochemical studies of Fujii and co-workers, who found similar trends.¹²

Because the electrophilic reaction mechanism results in electron transfer from substrate to oxidant orbitals, these differences in the EAs of the four oxidants also affect the subsequent reaction mechanisms and reactivities with substrates. The transition state structures for these reactions, however, show dramatic differences in group spin densities, as displayed in Figure 7. Thus, generally the reaction proceeds

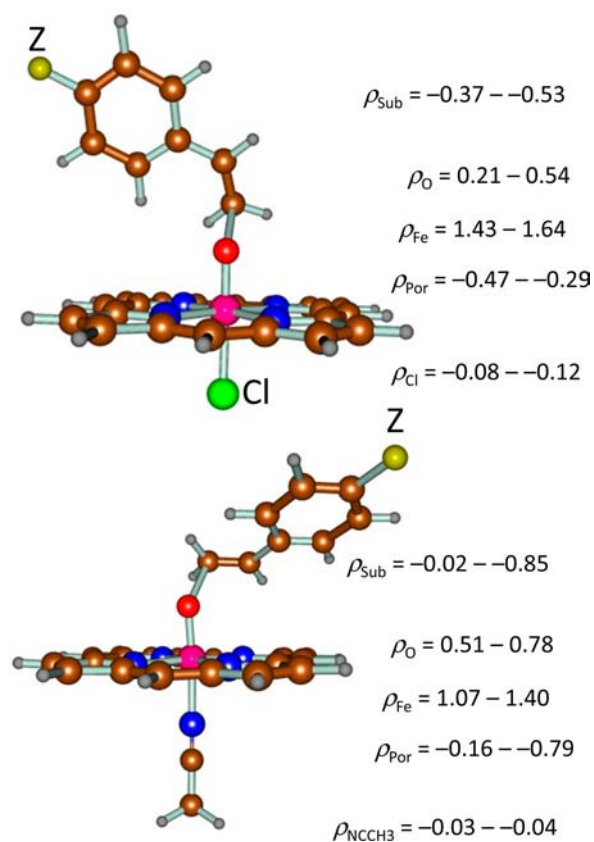


Figure 7. UB3LYP/BS2//UB3LYP/BS1-calculated group spin density ranges for *p*-Z-styrene epoxidation by **1**_{Cl} (top) and **1**_{AN} (bottom).

with electron transfer from the substrate to the half-filled a_{2u} porphyrin orbital, whereby a decrease in the spin density of the porphyrin group is found. The electronic configuration of the TS_{Cl,Z} structures is very much product-like with ρ_{Por} in the range from -0.29 to -0.47, whereas the TS_{AN,Z} values are reactant-like with considerably more spin density on the porphyrin ring.

Similarly, polarization of the FeO spin density from almost equal oxygen and iron spin densities in the reactants to a dominant iron radical in TS_{Cl,Z} occurs, whereby ρ_{Fe} ranges from 1.43 to 1.64 and ρ_{O} ranges from 0.21 to 0.54. By contrast, ρ_{Fe} varies from 1.07 to 1.40 and ρ_{O} ranges from 0.51 to 0.78 in the set of TS_{AN,Z} structures. The axial ligand, therefore, has an electronic effect on the charge and spin distributions in the rate-determining transition states, and, in particular, an anionic axial ligand, such as chloride, polarizes the FeO biradical toward the metal. Consequently, the anionic ligand will incur a “push” effect on the metal oxo group and formally change it from an Fe^VO^{•+} configuration in the reactant state to Fe^{IV}O²⁻ in the transition state. By contrast, an iron(IV) oxo oxidant with a neutral axial ligand retains much larger radical character on the

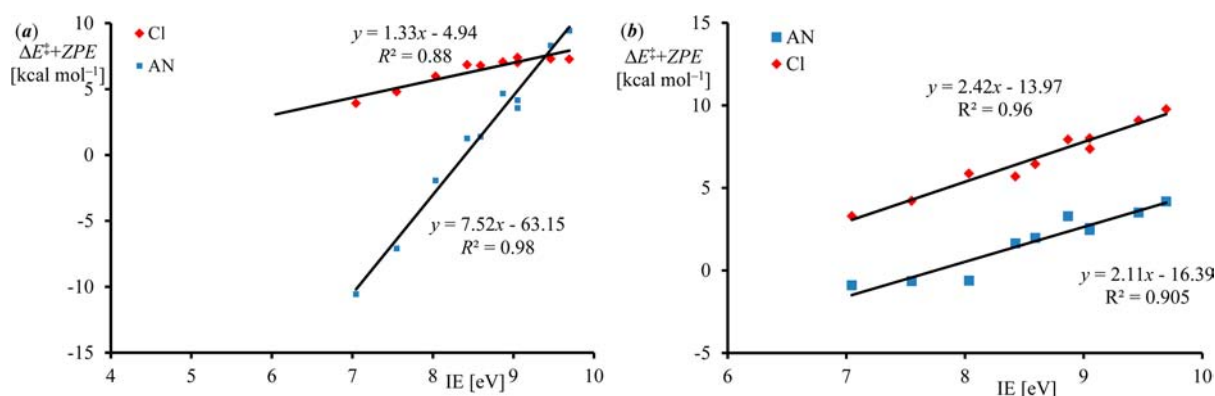


Figure 8. Styrene epoxidation barrier heights ($\Delta E^{\ddagger} + ZPE$) of ${}^2TS_{X,Z}$ plotted against the IE of the corresponding substrate. (a) Energies relative to isolated reactants. (b) Energies relative to a reactant complex (RC).

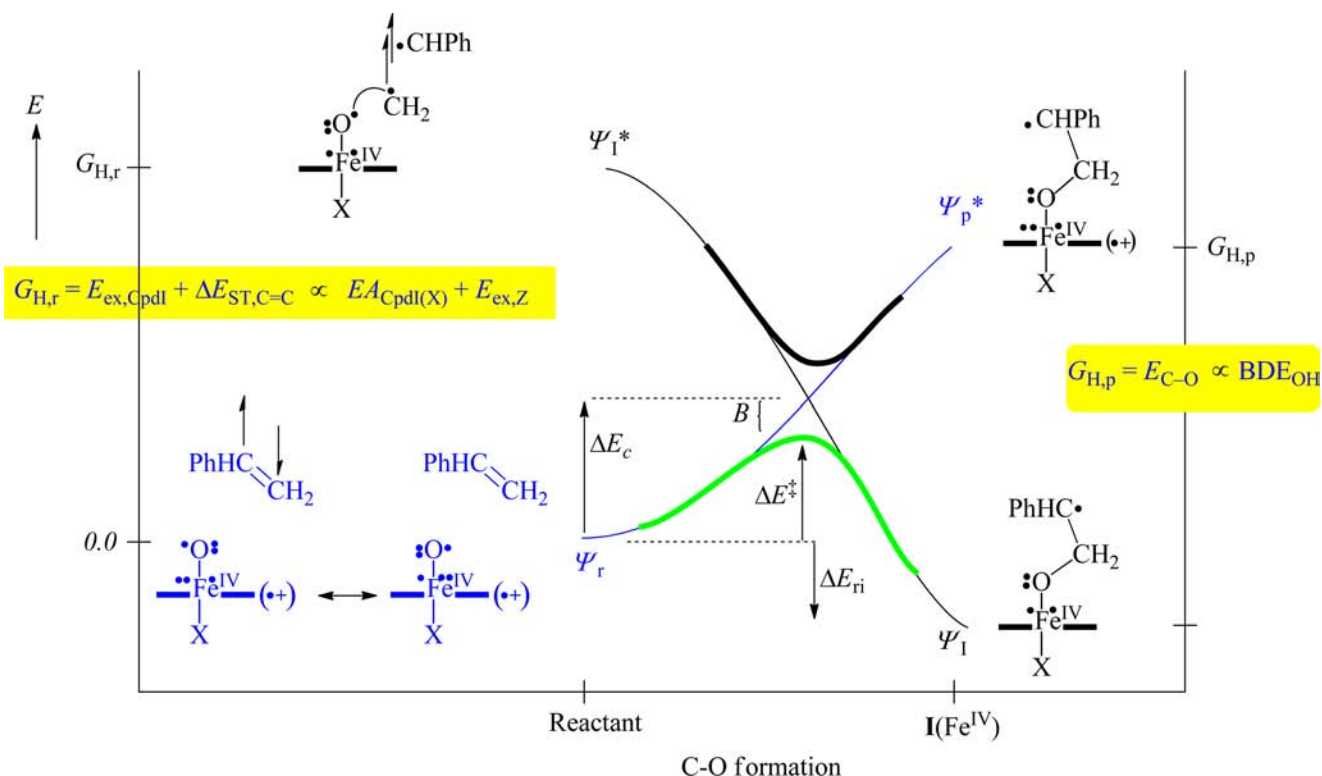


Figure 9. VB curve crossing diagram for *p*-Z-styrene epoxidation by iron(IV)-oxo porphyrin cation-radical oxidants. Lewis structures give relevant valence π orbitals with a dot.

oxygen atom in the electrophilic transition states and keeps the metal oxo group in a formal $Fe^{IV}O^{\bullet-}$ configuration. This is important because it reduces the barrier heights of the electrophilic reaction mechanisms.

Let us in the following look into the barrier heights of styrene epoxidation and elucidate the enthalpic contributions to the relative values of the associated rate constants. Experimental studies on substrate sulfoxidation by P450 enzymes indicated a correlation between the rate constants and IEs of the selected substrates.³¹ More recent mass spectrometric and computational studies showed that this correlation also applies to substrate epoxidation reactions.^{7s,10} To test this relationship for the set of data studied here, we plot in Figure 8 the calculated barrier heights ${}^2TS_{Cl,Z}$ and ${}^2TS_{AN,Z}$ as a function of the IEs of the *p*-Z-styrene substrates. We calculated the trends using two sets of relative energies: In the first, we take the isolated

reactants as a reference point, whereas in the second set, a reactant complex (RC) is used. DFT-calculated ionization potentials at the same level of theory as the transition states for the epoxidation reactions were used for consistency. Our calculated IE values are close to those reported in the literature;³² however, because not all IE values are experimentally known, we will use the calculated data in our analysis here. As can be seen, both series of *p*-Z-styrene epoxidation reactions give barriers that correlate linearly with the ionization potential, whether energies relative to isolated reactants or a reactant complex are used. Interestingly, the two correlations that use energies relative to isolated reactants have different slopes and intercepts, and indeed the two curves cross at an IE of about 9.40 eV. Therefore, $[Fe^{IV}(O)(Por^{\bullet+})NCCH_3]^+$ in the gas phase is a better oxidant than $[Fe^{IV}(O)(Por^{\bullet+})Cl]$ in epoxidation reactions with substrates with IE below 9.40 eV,

whereas it is reversed for substrates with higher ionization potentials, i.e., for *p*-CN-styrene and *p*-NO₂-styrene. This observation is in excellent agreement with the experimental studies of Nam et al.,¹¹ who also found improved reactivity of [Fe^{IV}(O)(Por^{•+})NCCH₃]⁺ over [Fe^{IV}(O)(Por^{•+})Cl] for the epoxidation of para-substituted styrenes with a large ρ^+ Hammett value of the substituent. The study that uses a reactant complex as the reference point, by contrast does not find this change in reactivity but instead produces almost parallel trends (Figure 8b). It may very well be, therefore, that the reactant complexes are unrealistic models and do not compare well with the experiment. Thus, in a reactant complex, the structures of the oxidant and substrate are solvated by solvent molecules and the interactions between all particles. In our reactant complex, no solvent molecules were included, and as a consequence, full freedom of optimization was possible, which may have resulted in an experimentally unrealistic structure.

To further understand the reactivity trends and the effect of the substrate and oxidant on the obtained barrier heights and, by extension, the rate constants, we set up a valence bond (VB) curve crossing diagram for styrene epoxidation by iron(IV)-oxo porphyrin cation-radical systems (Figure 9). The VB curve crossing diagram displayed here is analogous to that presented before for hydrogen-atom-abstraction reactions by iron(IV) oxo oxidants³³ but is further generalized to accommodate substrate epoxidation reactions.

This diagram starts on the bottom-left with the reactant configurations, i.e., styrene and [Fe^{IV}(O)(Por^{•+})X]. The latter appears in two VB configurations, where we highlight the valence π -orbital electrons with dots. Thus, the electronic ground state of [Fe^{IV}(O)(Por^{•+})X] is $\delta_{x^2-y^2}^2 \pi_{xz}^2 \pi_{yz}^2 \pi_{xz}^* \pi_{yz}^* 1a_{2u}^1$ in both the quartet and doublet spin states, and its wave function is labeled as Ψ_r in Figure 9. The $\delta_{x^2-y^2}$ orbital is a nonbonding orbital in the plane of the porphyrin ring. The perpendicular set of orbitals, π_{xz}/π_{xz}^* and π_{yz}/π_{yz}^* are the bonding and antibonding combinations of the metal 3d_{xz}/3d_{yz} with the oxygen 2p_x/2p_y atomic orbitals and contain three electrons in each pair.

In the C–O bond-formation step in the epoxidation mechanism, one electron is transferred from the substrate to the oxidant and it fills the a_{2u} orbital with a second electron to give the radical intermediate wave function Ψ_I . In VB theory,³³ the reactant (Ψ_r) and product (Ψ_I) wave functions cross each other and connect to excited states in the product and reactant conformations, respectively. Thus, Ψ_I^* is an excited reactant state with an electronic configuration that represents a C–O bond pair, a radical on the styrene group, and a closed-shell a_{2u} orbital. The two VB curves give an avoided crossing and a barrier height for C–O bond formation, ΔE^\ddagger . On the basis of a series of hydrogen-atom-abstraction reactions,^{33,34} it was shown that ΔE^\ddagger is proportional to the curve crossing energy (ΔE_c) minus the resonance energy *B* via $\Delta E^\ddagger = \Delta E_c - B$. However, the curve crossing energy is proportional to the promotion gap ($G_{H,r}$) or excitation energy from the reactant to product configuration in the geometry of the reactants so that the barrier height can be written as

$$\Delta E^\ddagger = fG_{H,r} - B \quad (1)$$

In a recent study, we showed that the relationship in eq 1 is also valid for substrate epoxidation and sulfoxidation reactions

and that the promotion gap $G_{H,r}$ reflects the excitation energy or ionization potential of the substrate.^{10,35}

A comparison of the VB structures for the Ψ_r and Ψ_I^* configurations shows that there is an electron transfer from the iron(IV) oxo group to the porphyrin a_{2u} orbital, reflecting an electron excitation in Cpdl ($E_{ex,Cpdl}$), which can be approximated with the EA of the oxidant. In addition, it can be seen that the electrons in the C=C bond are singlet-paired in the reactant ground state but triplet-coupled in the excited state in the reactant geometry, which implies a singlet–triplet energy gap in the C=C bond, ΔE_{ST} . Thus, a singlet–triplet energy gap in the C=C bond reflects the excitation energy of an electron in the π bond of the C=C moiety, namely, $E_{ex,Z}$, which, in turn, can be approximated with the IE of the substrate. Consequently, $G_{H,r}$ is proportional to $EA_{Cpdl(X)} + E_{ex,Z}$ and so should the barrier height of the epoxidation reaction. Of course, electron excitation from the π orbital of the substrate, which is the highest occupied molecular orbital, is also proportional to the IE of the substrate. Indeed, the plot in Figure 8 confirms a relationship between the barrier height and ionization potential, as predicted by the VB diagram in Figure 9.

For the reverse reaction, that is, from radical intermediates to reactants, the epoxidation barrier height (ΔE_{rev}^\ddagger) is equal to ΔE^\ddagger plus the exothermicity to form radical intermediates (ΔE_n). In VB, the reverse barrier is proportional to the promotion gap in the radical intermediates, i.e., Ψ_I to Ψ_p^* or $G_{H,p}$. The VB structures on the radical intermediate side of Figure 9 show that the excitation energy $G_{H,p}$ corresponds to the formation energy of the C–O bond plus the electron transfer from the substrate into the a_{2u} orbital. The VB structures in Figure 9 indicate that the electrons in the C–O bond are singlet-coupled in Ψ_I but triplet-coupled in Ψ_p^* , which implies that a singlet–triplet excitation in the C–O bond has occurred. The singlet–triplet excitation in the C–O bond refers to the bond breaking of the C–O bond. In earlier work, we showed that the C–O bond-formation energy is proportional to a H–O bond-formation energy, so that it can be mimicked with BDE_{OH}, defined as the reaction enthalpy for eq 2.¹⁰

To test whether the VB curve crossing diagram can predict the barrier heights from empirical values, we calculated the gas-phase EAs of all four oxidants from Figure 1 and the π – π^* excitation energies and IEs of all *p*-Z-styrene substrates, and the results are given in Table 1. We calculated the EA of the

Table 1. Substrate Chemical Properties and Charge-Transfer (Q_{CT}) Values in the Transition States

Z	IE _Z ^a	$E_{ex,Z}$ ^a	$Q_{CT,Cl}$ ^b	$Q_{CT,AN}$ ^c
H	9.05	3.82	0.10	0.25
F	9.05	3.81	0.07	0.24
Cl	8.87	3.70	0.08	0.16
CH ₃	8.59	3.75	0.12	0.32
<i>t</i> -Bu	8.43	3.76	0.12	0.42
CN	9.46	3.46	0.01	0.10
NO ₂	9.70	2.88	−0.03	−0.01
OCH ₃	8.03	3.73	0.16	0.42
NH ₂	7.55	3.61	0.22	0.55
N(CH ₃) ₂	7.05	3.57	0.27	0.63

^aIn electronvolts. ^bCharge transfer in ²TS_{Cl,Z}. ^cCharge transfer in ²TS_{AN,Z}.

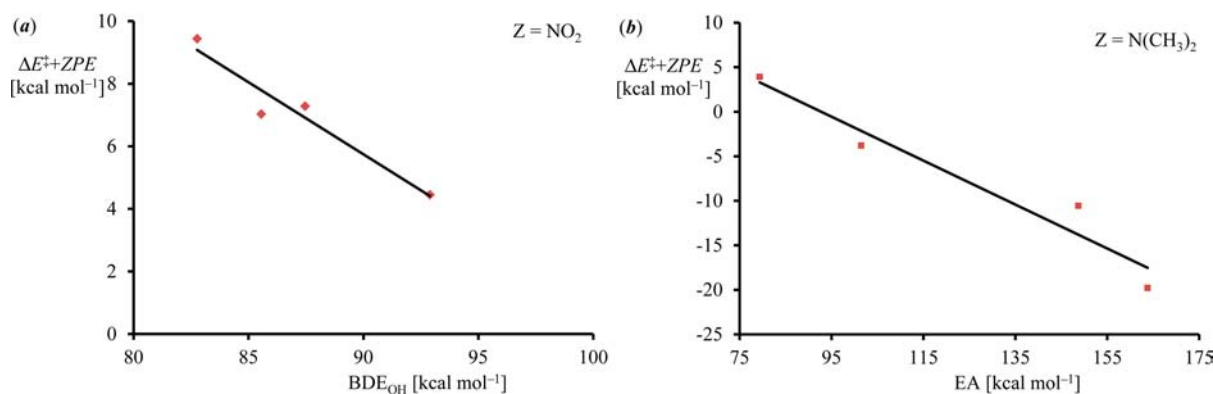
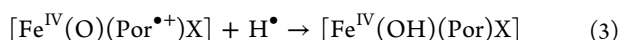


Figure 10. Correlations of (a) the epoxidation barrier height of *p*-NO₂-styrene with BDE_{OH} and (b) the epoxidation barrier height of *p*-N(CH₃)₂-styrene with $EA_{CpdI(X)}$.

oxidant, the π - π^* excitation energy in the *p*-*Z*-styrene substrates, and the promotion gap via eq 2. Subsequently, we used these values to estimate ΔE_{VB}^{\ddagger} for all substrates. Although these VB-calculated barrier heights are, on average, within -0.05 kcal mol⁻¹ of the DFT-calculated ones, actually the standard deviation is quite large (about 2 kcal mol⁻¹). This implies that the model has shortcomings, which we address with a slightly modified model as described below.

$$G_{H,r} = 2(EA_{CpdI(X)} + E_{ex,Z}) \quad (2)$$



Thus, the forward reaction barrier is dependent on the intrinsic chemical properties of the substrate, i.e., the IE, whereas the reverse reaction barrier depends on the variables of the oxidant, i.e., the BDE_{OH} value. We calculated gas-phase values of $BDE_{OH} = 87.5$ kcal mol⁻¹ for $[Fe^{IV}(O)(Por^{\bullet+})Cl]$ and $BDE_{OH} = 82.8$ kcal mol⁻¹ for $[Fe^{IV}(O)(Por^{\bullet+})NCCH_3]^+$, respectively.²³ This energy difference narrows to almost equal values in a dielectric constant of $\epsilon = 5.7$: $BDE_{OH} = 82.3$ and 81.3 kcal mol⁻¹ for $[Fe^{IV}(O)(Por^{\bullet+})X]$, $X = Cl^-$ or $NCCH_3$, respectively.

The VB diagram of Figure 9 shows that the transition state described from reactants to intermediates, i.e., forward, is proportional to $EA_{CpdI(X)} + E_{ex,Z}$, whereas the transition state in the reverse reaction, i.e., backward, is proportional to the BDE_{OH} value of the oxidant. Thus, the location of the barrier on the potential energy surface will determine whether the barrier correlates with $EA_{CpdI(X)} + E_{ex,Z}$ or BDE_{OH} . So, for a substrate epoxidation reaction where the transition state has a very reactant-like electronic configuration, i.e., an early transition state, very little electron transfer from the substrate to the oxidant has taken place and consequently the reactant wave function dominates in the transition state. As a result, an early transition state should be proportional to BDE_{OH} . On the other hand, a late transition state has an electronic configuration closely resembling the radical intermediate state because of a significant amount of electron transfer that has taken place already. Therefore, late transition states, based on the VB diagram in Figure 8, should correlate with the EA of the oxidant. Indeed, the group spin density of the epoxidation transition state with *p*-NO₂-styrene as a substrate shows only a small amount of electron transfer from the substrate to the oxidant, and consequently the charge transfer from the substrate to the oxidant (Q_{CT}) is almost zero. This implies that the epoxidation barriers for *p*-NO₂-styrene will be early on

the potential energy surface, and little electron transfer has taken place. As reasoned above, these barrier heights should, therefore, correlate with BDE_{OH} and not with $EA_{CpdI(X)} + E_{ex,Z}$. To test this, we display in Figure 10 the correlation of *p*-NO₂-styrene epoxidation with BDE_{OH} for $1_X/2_X$ ($X = Cl^-$ and $NCCH_3$). As can be seen for this set of four data points, a linear correlation is found between the epoxidation barrier of *p*-NO₂-styrene and the corresponding BDE_{OH} value of the oxidant.

The group spin densities of ${}^2TS_{X,N(CH_3)_2}$ in contrast to those found for ${}^2TS_{X,NO_2}$, show considerably larger amounts of spin density on the substrate part of the structure. At the same time, the spin density on the porphyrin ring has dropped because of electron transfer from the substrate to the oxidant. Thus, the ${}^2TS_{X,N(CH_3)_2}$ structures are electronically late and resemble product-type conformations. Because of that, in ${}^2TS_{X,N(CH_3)_2}$ electron transfer has taken place already (or at least most of it) and, consequently, the barrier height will be driven by the differences in the EAs of the individual oxidants. To test this, we plot in Figure 10b the correlation between the epoxidation barrier height of *p*-N(CH₃)₂-styrene epoxidation by $1_X/2_X$ oxidants as a function of the EA of the oxidant. We find a linear correlation between the EA and barrier height, as predicted by the VB diagram in Figure 8.

As follows from the correlations depicted in Figure 10, the amount of electron transfer from the substrate to the oxidant determines whether a transition state correlates either with the sum of $EA_{CpdI(X)} + E_{ex,Z}$ or with BDE_{OH} instead. Thus, we extracted the degree of charge transfer from the substrate to the oxidant (Q_{CT}) from the UB3LYP/B2//UB3LYP/B1 calculations and summarize these values for the ${}^2TS_{X,Z}$ transition states in Table 1. We now define the variable ω , which describes the position of the transition state on the potential energy profile through eq 4, and link ω to the degree of charge transfer (Q_{CT}), BDE_{OH} , and $EA_{CpdI(X)} + E_{ex,Z}$.

$$\omega = Q_{CT}BDE_{OH} + (1 - Q_{CT})(EA_{CpdI(X)} + E_{ex,Z}) \quad (4)$$

Essentially, ω is proportional to BDE_{OH} when the charge transfer is maximal, i.e., an early transition state, but it is proportional to $EA_{CpdI(X)} + E_{ex,Z}$ for a late transition state with a small value of Q_{CT} . We calculated ω for all transition states ${}^2TS_{X,Z}$, $X = Cl^-/NCCH_3$ and *p*-*Z*-styrene as substrates, and a plot of all data is given in Figure 11. Thus, the full set of transition states, irrespective of the axial ligand of the oxidant, fits a linear correlation. Consequently, we described the trend in epoxidation barriers for early as well as late transition states

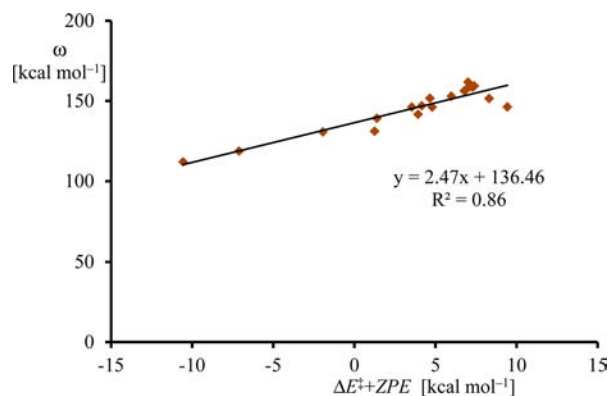


Figure 11. Correlation between the epoxidation barrier height of all data for I_X ($X = \text{Cl}^-$, NCCCH_3) with parameter ω .

as a function of the intrinsic chemical properties of the oxidant and substrate and the amount of charge transfer in the TS during the reaction process.

In summary, we show here that the barrier height of an epoxidation reaction by a metal oxo oxidant is dependent on the electron-donating/withdrawing character of the substituents of the substrate. Thus, substrates with high electron-donating power such as *p*- $\text{N}(\text{CH}_3)_2$ -styrene result in low barrier heights and rapid electron transfer from the substrate to the oxidant well before the epoxidation barrier height has been overcome. On the other hand, electron-withdrawing groups such as *p*- NO_2 -styrene result in much later electron transfer from the substrate to the oxidant, and now the height of the barrier is determined by the strength of the C–O bond that is formed.

CONCLUSIONS

In this work, we report a systematic computational study into substrate epoxidation by four iron(IV)-oxo porphyrin cation-radical models. We investigated the effect of the axial ligand, chloride versus acetonitrile, as well as the equatorial ligand, Por versus TPFPP. It is shown that the substituents on the porphyrin ring can guide substrate binding through electrostatic interactions with halide atoms, which lowers the barrier heights. A neutral axial ligand leads to displacement of the metal from the plane through the porphyrin ring and results in different orbital interactions between the metal and porphyrin ring compared to systems with an anionic ligand. This has profound effects on the EA of the oxidant and the subsequent reactivity patterns. Finally, we investigated *p*-*Z*-styrene epoxidation by four iron(IV)-oxo porphyrin cation-radical models and highlight the differences in reactivity for olefins with electron-withdrawing versus electron-donating substituents. In particular, it is shown that electron-donating substituents give early transition states and lower reaction barriers than substrates with electron-withdrawing substituents.

ASSOCIATED CONTENT

Supporting Information

Tables with group spin densities, charges, and relative energies of all complexes described in this work as well as Cartesian coordinates of all optimized geometries. This material is available free of charge via the Internet at <http://pubs.acs.org>.

AUTHOR INFORMATION

Corresponding Author

*E-mail: sam.devisser@manchester.ac.uk (S.P.d.V.), dkclcre@yahoo.com (D.K.), rezalatifi@gmail.com (R.L.).

Notes

The authors declare no competing financial interest.

ACKNOWLEDGMENTS

The research was supported by the CPU time provided by the National Service of Computational Chemistry Software. D.K. is Ramanujan Fellow of the Department of Science and Technology, New Delhi, India (Research Grants SR/S2/RJN-11/2008), and also acknowledges financial support from the OSDD unit of the Council of Scientific & Industrial Research, New Delhi, India (Grant OSDD/HCP0001/12FYP/2012-13/Fin/2455). M.A.S. thanks the Petroleum Technology Development Fund of the Nigerian Government for a scholarship. E.V.R.-A. thanks the U.S. Department of Energy, Office of Basic Energy Science (Grant DE-FG02-06ER15799).

REFERENCES

- (1) (a) Sono, M.; Roach, M. P.; Coulter, E. D.; Dawson, J. H. *Chem. Rev.* **1996**, *96*, 2841–2888. (b) Groves, J. T. *Proc. Natl. Acad. Sci. U.S.A.* **2003**, *100*, 3569–3574. (c) Ortiz de Montellano, P. R., Ed. *Cytochrome P450: Structure, Mechanism and Biochemistry*, 3rd ed.; Kluwer Academic/Plenum Publishers: New York, 2004. (d) Kadish, K. M., Smith, K. M., Guillard, R., Eds. *Handbook of Porphyrin Science*; World Scientific Publishing Co.: New York, 2010. (e) Ortiz de Montellano, P. R. *Chem. Rev.* **2010**, *110*, 932–948. (f) de Visser, S. P., Kumar, D., Eds. *Iron-containing enzymes: Versatile catalysts of hydroxylation reactions in nature*; RSC Publishing: Cambridge, U.K., 2011.
- (2) (a) Denisov, I. G.; Makris, T. M.; Sligar, S. G.; Schlichting, I. *Chem. Rev.* **2005**, *105*, 2253–2277. (b) Rittle, J.; Green, M. T. *Science* **2010**, *330*, 933–937.
- (3) (a) Groves, J. T.; Shalyaev, K.; Lee, J. In *The Porphyrin Handbook*; Kadish, K. M., Smith, K. M., Guillard, R., Eds.; Academic Press: New York, 2000; Vol. 4, Chapter 27, pp 17–40. (b) Nam, W. *Acc. Chem. Res.* **2007**, *40*, 522–531.
- (4) (a) Ruettinger, R. T.; Fulco, A. J. *J. Biol. Chem.* **1981**, *256*, 5728–5734. (b) Guengerich, F. P. *Arch. Biochem. Biophys.* **2003**, *409*, 59–71. (c) McLean, K. J.; Munro, A. W. *Drug Metabol. Rev.* **2008**, *40*, 427–446.
- (5) (a) Groves, J. T.; Avaria-Neisser, G. E.; Fish, K. M.; Imachi, M.; Kuczkowski, R. L. *J. Am. Chem. Soc.* **1986**, *108*, 3837–3838. (b) Alcalde, M.; Farinas, E. T.; Arnold, F. H. *J. Biomol. Screen.* **2004**, *9*, 141–146. (c) Dansette, P. M.; Bertho, G.; Mansuy, D. *Biochem. Biophys. Res. Commun.* **2005**, *338*, 450–455. (d) Yuan, X.; Wang, Q.; Horner, J. H.; Sheng, X.; Newcomb, M. *Biochemistry* **2009**, *48*, 9140–9146. (e) Shinkyu, R.; Xu, L.; Tallman, K. A.; Cheng, Q.; Porter, N. A.; Guengerich, T. P. *J. Biol. Chem.* **2011**, *286*, 33021–33028.
- (6) Ortiz de Montellano, P. R.; Fruetel, J. A.; Collins, J. R.; Campere, D. L.; Loew, G. H. *J. Am. Chem. Soc.* **1991**, *113*, 3195–3196.
- (7) For example, see: (a) Groves, J. T.; Myers, R. S. *J. Am. Chem. Soc.* **1983**, *105*, 5791–5796. (b) Groves, J. T.; Watanabe, Y. *J. Am. Chem. Soc.* **1986**, *108*, 507–508. (c) Collman, J. P.; Kodadek, T.; Brauman, J. I. *J. Am. Chem. Soc.* **1986**, *108*, 2588–2594. (d) Ostović, D.; Bruce, T. C. *J. Am. Chem. Soc.* **1989**, *111*, 6511–6517. (e) Collman, J. P.; Brauman, J. I.; Hampton, P. D.; Tanaka, H.; Bohle, D. S.; Hembre, R. T. *J. Am. Chem. Soc.* **1990**, *112*, 7980–7984. (f) Groves, J. T.; Gross, Z.; Stern, M. K. *Inorg. Chem.* **1994**, *33*, 5065–5072. (g) Stephenson, N. A.; Bell, A. T. *Inorg. Chem.* **2006**, *45*, 2758–2766. (h) Collman, J. P.; Zeng, L.; Wang, H. J. H.; Lei, A.; Brauman, J. I. *Eur. J. Org. Chem.* **2006**, 2707–2714. (i) Hessnauer-Ilicheva, N.; Franke, A.; Meyer, D.; Woggon, W.-D.; van Eldik, R. *J. Am. Chem. Soc.* **2007**, *129*, 12473–12479. (j) Mas-Balleste, R.; Que, L., Jr. *J. Am. Chem. Soc.* **2007**, *129*,

- 15964–15972. (k) Comba, P.; Rajaraman, G. *Inorg. Chem.* **2008**, *47*, 78–93. (l) Bruijninx, P. C. A.; Buurmans, I. L. C.; Gosiewska, S.; Moelands, M. A. H.; Lutz, M.; Spek, A. L.; van Koten, G.; Klein Gebbink, R. J. M. *Chem.—Eur. J.* **2008**, *14*, 1228–1237. (m) Hull, J. F.; Sauer, E. L. O.; Incarvito, C. D.; Faller, J. W.; Brudvig, G. W.; Crabtree, R. H. *Inorg. Chem.* **2009**, *48*, 488–495. (n) McGown, A. J.; Kerber, W. D.; Fujii, H.; Goldberg, D. P. *J. Am. Chem. Soc.* **2009**, *131*, 8040–8048. (o) Company, A.; Feng, Y.; Güell, M.; Ribas, X.; Luis, J. M.; Que, L., Jr.; Costas, M. *Chem.—Eur. J.* **2009**, *15*, 3359–3362. (p) Franke, A.; Wolak, M.; van Eldik, R. *Chem.—Eur. J.* **2009**, *15*, 10182–10198. (q) Hessnauer-Ilicheva, N.; Franke, A.; Wolak, M.; Higuchi, T.; van Eldik, R. *Chem.—Eur. J.* **2009**, *15*, 12447–12459. (r) Leeladee, P.; Goldberg, D. P. *Inorg. Chem.* **2010**, *49*, 3083–3085. (s) Lanucara, F.; Crestoni, M. E. *Chem.—Eur. J.* **2011**, *17*, 12092–12100.
- (8) (a) Gross, Z.; Nimri, S. *Inorg. Chem.* **1994**, *33*, 1731–1732. (b) Gross, Z. *J. Biol. Inorg. Chem.* **1996**, *1*, 368–371. (c) Czarnecki, K.; Nimri, S.; Gross, Z.; Proniewicz, L. M.; Kincaid, J. R. *J. Am. Chem. Soc.* **1996**, *118*, 2929–2935.
- (9) Green, M. T.; Dawson, J. H.; Gray, H. B. *Science* **2004**, *304*, 1653–1656.
- (10) Kumar, D.; Karamzadeh, B.; Sastry, G. N.; de Visser, S. P. *J. Am. Chem. Soc.* **2010**, *132*, 7656–7667.
- (11) Song, W. J.; Ryu, Y. O.; Song, R.; Nam, W. *J. Biol. Inorg. Chem.* **2005**, *10*, 294–304.
- (12) (a) Takahashi, A.; Kurahashi, T.; Fujii, H. *Inorg. Chem.* **2011**, *50*, 6922–6928. (b) Cong, Z.; Kurahashi, T.; Fujii, H. *Angew. Chem., Int. Ed.* **2011**, *50*, 9935–9939.
- (13) (a) *Jaguar*, version 7.9; Schrödinger, LLC: New York, 2011. (b) Frisch, M. J.; et al. *Gaussian03*, revision C.01; Gaussian, Inc.: Wallingford, CT, 2004. (c) Frisch, M. J.; et al. *Gaussian09*, revision A.1; Gaussian, Inc.: Wallingford, CT, 2009.
- (14) (a) Becke, A. D. *J. Chem. Phys.* **1993**, *98*, 5648–5652. (b) Lee, C.; Yang, W.; Parr, R. G. *Phys. Rev. B* **1988**, *37*, 785–789.
- (15) (a) Hay, P. J.; Wadt, W. R. *J. Chem. Phys.* **1985**, *82*, 270–283. (b) Hehre, W. J.; Ditchfield, R.; Pople, J. A. *J. Chem. Phys.* **1972**, *56*, 2257–2261.
- (16) (a) de Visser, S. P.; Oh, K.; Han, A.-R.; Nam, W. *Inorg. Chem.* **2007**, *46*, 4632–4641. (b) Vardhaman, A. K.; Sastri, C. V.; Kumar, D.; de Visser, S. P. *Chem. Commun.* **2011**, *47*, 11044–11046.
- (17) de Visser, S. P. *J. Am. Chem. Soc.* **2010**, *132*, 1087–1097.
- (18) Schwabe, T.; Grimme, S. *Phys. Chem. Chem. Phys.* **2007**, *9*, 3397–3406.
- (19) Reiher, M.; Salomon, O.; Hess, B. A. *Theor. Chem. Acc.* **2001**, *107*, 48–55.
- (20) Kumar, D.; Thiel, W.; de Visser, S. P. *J. Am. Chem. Soc.* **2011**, *133*, 3869–3882.
- (21) (a) Green, M. T. *J. Am. Chem. Soc.* **1999**, *121*, 7939–7940. (b) Ogliaro, F.; de Visser, S. P.; Cohen, S.; Kaneti, J.; Shaik, S. *ChemBioChem* **2001**, *11*, 848–851. (c) Kamachi, T.; Yoshizawa, K. *J. Am. Chem. Soc.* **2003**, *125*, 4652–4661. (d) Bathelt, C. M.; Zurek, J.; Mulholland, A. J.; Harvey, J. N. *J. Am. Chem. Soc.* **2005**, *127*, 12900–12908. (e) Lonsdale, R.; Oláh, J.; Mulholland, A. J.; Harvey, J. N. *J. Am. Chem. Soc.* **2011**, *133*, 15464–15474. (f) Isobe, H.; Yamanaka, S.; Okumura, M.; Yamaguchi, K.; Shimada, J. *J. Phys. Chem. B* **2011**, *115*, 10730–10738.
- (22) Shaik, S.; Kumar, D.; de Visser, S. P.; Altun, A.; Thiel, W. *Chem. Rev.* **2005**, *105*, 2279–2328.
- (23) de Visser, S. P.; Tahsini, L.; Nam, W. *Chem.—Eur. J.* **2009**, *15*, 5577–5587.
- (24) de Visser, S. P.; Shaik, S.; Sharma, P. K.; Kumar, D.; Thiel, W. *J. Am. Chem. Soc.* **2003**, *125*, 15779–15788.
- (25) (a) Linde, C.; Åkermark, B.; Norrby, P.-O.; Svensson, M. *J. Am. Chem. Soc.* **1999**, *121*, 5083–5084. (b) Kamachi, T.; Shiota, Y.; Ohta, T.; Yoshizawa, K. *Bull. Chem. Soc. Jpn.* **2003**, *76*, 721–732. (c) Quiñero, D.; Musaev, D. G.; Morokuma, K. *Inorg. Chem.* **2003**, *42*, 8449–8455. (d) Sharma, P. K.; de Visser, S. P.; Ogliaro, F.; Shaik, S. *J. Am. Chem. Soc.* **2003**, *125*, 2291–2300. (e) Hirao, H.; Kumar, D.; Thiel, W.; Shaik, S. *J. Am. Chem. Soc.* **2005**, *127*, 13007–
13018. (f) Kumar, D.; Derat, E.; Khenkin, A. M.; Neumann, R.; Shaik, S. *J. Am. Chem. Soc.* **2005**, *127*, 17712–17718. (g) Bassan, A.; Blomberg, M. R. A.; Siegbahn, P. E. M.; Que, L., Jr. *Angew. Chem., Int. Ed.* **2005**, *44*, 2939–2941.
- (26) (a) de Visser, S. P.; Ogliaro, F.; Harris, N.; Shaik, S. *J. Am. Chem. Soc.* **2001**, *123*, 3037–3047. (b) de Visser, S. P.; Ogliaro, F.; Shaik, S. *Angew. Chem., Int. Ed.* **2001**, *40*, 2871–2874. (c) de Visser, S. P.; Ogliaro, F.; Sharma, P. K.; Shaik, S. *Angew. Chem., Int. Ed.* **2002**, *41*, 1947–1951. (d) de Visser, S. P.; Ogliaro, F.; Sharma, P. K.; Shaik, S. *J. Am. Chem. Soc.* **2002**, *124*, 11809–11826. (e) Kumar, D.; de Visser, S. P.; Shaik, S. *Chem.—Eur. J.* **2005**, *11*, 2825–2835.
- (27) (a) Kumar, D.; de Visser, S. P.; Shaik, S. *J. Am. Chem. Soc.* **2003**, *125*, 13024–13025. (b) Kumar, D.; de Visser, S. P.; Sharma, P. K.; Cohen, S.; Shaik, S. *J. Am. Chem. Soc.* **2004**, *126*, 1907–1920. (c) Kumar, D.; de Visser, S. P.; Shaik, S. *J. Am. Chem. Soc.* **2004**, *126*, 5072–5073. (d) de Visser, S. P. *Chem.—Eur. J.* **2006**, *12*, 8168–8177.
- (28) (a) Ben-Daniel, R.; de Visser, S. P.; Shaik, S.; Neumann, R. *J. Am. Chem. Soc.* **2003**, *125*, 12116–12117. (b) de Visser, S. P.; Kaneti, J.; Neumann, R.; Shaik, S. *J. Org. Chem.* **2003**, *68*, 2903–2912.
- (29) Kumar, D.; Tahsini, L.; de Visser, S. P.; Kang, H. Y.; Kim, S. J.; Nam, W. *J. Phys. Chem. A* **2009**, *113*, 11713–11722.
- (30) de Visser, S. P. *J. Am. Chem. Soc.* **2006**, *128*, 15809–15818.
- (31) (a) Watanabe, Y.; Iyanagi, T.; Oae, S. *Tetrahedron Lett.* **1980**, *21*, 3685–3688. (b) Watanabe, Y.; Numata, T.; Iyanagi, T.; Oae, S. *Bull. Chem. Soc. Jpn.* **1981**, *54*, 1163–1170. (c) Watanabe, Y.; Iyanagi, T.; Oae, S. *Tetrahedron Lett.* **1982**, *23*, 533–536.
- (32) Lide, D. R. *CRC Handbook of Chemistry and Physics*, 76th ed.; CRC Press: Boca Raton, FL, 1996.
- (33) Shaik, S. S. *J. Am. Chem. Soc.* **1981**, *103*, 3692–3701.
- (34) (a) Shaik, S.; Kumar, D.; de Visser, S. P. *J. Am. Chem. Soc.* **2008**, *130*, 10128–10140. (b) Latifi, R.; Bagherzadeh, L.; de Visser, S. P. *Chem.—Eur. J.* **2009**, *15*, 6651–6662.
- (35) Kumar, D.; Sastry, G. N.; de Visser, S. P. *Chem.—Eur. J.* **2011**, *17*, 6196–6205.